Theory of epsilon-near-zero modes in ultrathin films

Salvatore Campione, Igal Brener, and Francois Marquier

Theory of epsilon-near-zero modes in ultra-thin films

Salvatore Campione,[1,2,*] Igal Brener,[1,2] and Francois Marquier[3,*]

[1]*Center for Integrated Nanotechnologies (CINT), Sandia National Laboratories, P.O. Box 5800, Albuquerque, NM 87185, USA*
[2]*Sandia National Laboratories, P.O. Box 5800, Albuquerque, NM 87185, USA*
[3]*Laboratoire Charles Fabry, Institut d Optique, CNRS–Univ Paris-Sud, Campus Polytechnique, RD128, 91127 Palaiseau Cedex, France*
[*]*sncampi@sandia.gov, francois.marquier@institutoptique.fr*

The physics of the epsilon-near-zero (ENZ) mode, which is supported by a nanolayer at the frequency where the dielectric permittivity vanishes, has recently been a subject of debate. In this paper, we thoroughly investigate and clarify the physics of this mode, providing its main characteristics and its domain of existence. This understanding will benefit all the applications that rely on ENZ modes in semiconductor nanolayers, including directional perfect absorption, voltage-tunable devices, and ultrafast thermal emission.

PACS numbers: 78.20.-e; 78.20.Bh; 78.67.-n

Thin films made of metals, doped semiconductors or polar materials can support plasmon- or phonon-polaritons eigenmodes [1-4]. For excitation conditions close to the dispersion of such eigenmodes, these structures can exhibit peculiar properties. A representative example is the Berreman absorption feature observed for *p*-polarized light illuminating dielectric thin films backed by a metal substrate [5-7]. This resonant absorption, close to the longitudinal phonon frequency, was recently attributed to the excitation of the so-called "Berreman mode" [8]. On thin plasmonic films, the same resonant absorption occurs near the plasma frequency and was attributed to a "Brewster mode" [9], whose dispersion was recently proven experimentally in [10]. These modes are radiative modes: their dispersion relation lies on the left of the light line and thus can be excited from free-space. The physics of such modes is well understood [11-15]: they appear when the dielectric constant is close to zero and are associated with a collective oscillation of charges in the thin films.

Very recently, another mode – defined as the "epsilon-near-zero" (ENZ) mode – was observed in [8] and only when very subwavelength film thicknesses were used. This ENZ mode is a confined mode whose dispersion lies on the right of the light line and thus can be accessed using the Kretschmann geometry or grating couplers, for example. It was briefly shown that this mode corresponds to a long-range surface wave mode in the thin-film regime [16]. However, a clear theoretical investigation of the behavior and domain of existence of the ENZ mode has not been reported yet, and it is the purpose of this work. The understanding of the physics of the ENZ mode will benefit all the applications that could rely on it [17], such as directional perfect absorption and ultrafast thermal emission.

We will consider in this paper the three-layer structure depicted in Fig. 1, where a nanolayer with thickness d and relative permittivity ε_2 is surrounded by two semi-infinite regions with relative permittivities ε_1 (top) and ε_3 (bottom).
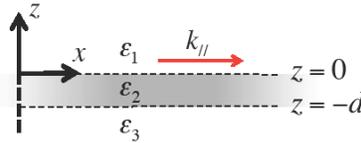
Fig. 1. A three-layer structure containing a layer with thickness d and two semi-infinite regions.

A solution to Maxwell's equations in the absence of excitation defines a *mode* of the structure. A mode is characterized by a pair $(k_{//}, \omega)$, that satisfies the equation

$$1 + \frac{\varepsilon_1 k_{z3}}{\varepsilon_3 k_{z1}} = i \tan(k_{z2}d)\left(\frac{\varepsilon_2 k_{z3}}{\varepsilon_3 k_{z2}} + \frac{\varepsilon_1 k_{z2}}{\varepsilon_2 k_{z1}}\right) \qquad (1)$$

where $k_{//}$ is the transverse wavenumber, ω the angular frequency, and $k_{zi}^2 = \varepsilon_i \frac{\omega^2}{c^2} - k_{//}^2$ is the longitudinal wavenumber in medium $i = 1,2,3$ with $\mathrm{Re}(k_{zi}) + \mathrm{Im}(k_{zi}) \geq 0$. Equation (1) can be easily derived from either the Fresnel reflection coefficient [18,19] or the transfer matrix method [20]. The monochromatic time harmonic

convention $\exp(-i\omega t)$ is implicitly assumed. Equation (1) deals with complex-valued variables and can be solved in two manners: (i) selecting a real-valued ω and computing the complex-valued $k_{//}$; or (ii) selecting a real-valued $k_{//}$ and computing the complex-valued ω. Both descriptions lead to different representations of the same mode but are equivalent as shown in [21]. We continue with description (ii) for the remainder of the paper as suggested in [1] and [8].

For the sake of simplicity, and in order to extract the essential physics of the ENZ mode, we consider a metallic nanolayer, whose dielectric constant is described by a simple Drude model $\varepsilon_2(\omega)=1-\dfrac{\omega_P^2}{\omega^2+i\gamma\omega}$, with ω_P depicting the plasma angular frequency and γ the damping, and surrounded by free space ($\varepsilon_1=\varepsilon_3=1$). The dielectric constant of the film can vanish when the frequency is close to ω_P, leading to the possibility to observe an ENZ mode. Unless otherwise indicated, $\omega_P=10000\,\text{cm}^{-1}$ (corresponding to a plasma wavelength $\lambda_P=1\mu m$) and $\gamma=100\,\text{cm}^{-1}$, and are used as representative examples for the figures shown in this paper. For the same reasons of simplicity, we will not address the issue of non-local effects that could arise from very small film thicknesses. More complex environments will be studied at the end of the paper. The plasmonic film supports surface plasmon polariton (SPP) modes. When its thickness d is larger than the skin depth, (~100 nm), the layer can be considered as a semi-infinite medium. This is clearly observed in Fig. 2(a), where we report the dispersion of the real part of ω of the SPP supported by a 1μm-thick slab in free space (blue curve). The figure displays the classic growing trend to the right of the light line, approaching $\text{Re}(\omega)/\omega_P=1/\sqrt{2}$ for large $k_{//}$. It is also known that when the thickness d is comparable to the skin depth, the SPP splits into the short-range SPP and the long-range SPP [22,23]. This is displayed in Fig. 2(b), where we show the dispersion relations of the two SPPs supported by a 100nm-thick slab. Similar to the case reported in Fig. 2(a), also the two SPPs in Fig. 2(b) approach $\text{Re}(\omega)/\omega_P=1/\sqrt{2}$ for large $k_{//}$.

However, limited discussion has been provided in the literature to the dispersion of short-range and long-range SPPs when the slab thickness is further reduced to values (much) smaller than the skin depth. Similar to what is reported in Fig. 2(b), Fig. 2(c) shows the dispersion relations of the two SPPs, but now for a 2nm-thick film (using the Drude values used before). In this case, we observe that the dispersion of the long-range SPP remains quite constant at $\text{Re}(\omega)/\omega_P=1$ for increasing $k_{//}$. Because of this peculiar condition, and although this is still a long-range SPP, this part of the dispersion has been defined as an ENZ mode. Plotting the same dispersion in a wider $k_{//}$ range [Fig. 2(d)] confirms the behavior of short-range and long-range SPPs observed in Fig. 2(b), i.e. ω approaches $\text{Re}(\omega)/\omega_P=1/\sqrt{2}$ for large $k_{//}$. Thus, we infer that the so-called ENZ mode can exist only for certain ranges of thickness, frequency, and wavenumber, and our first objective is to define theses ranges.
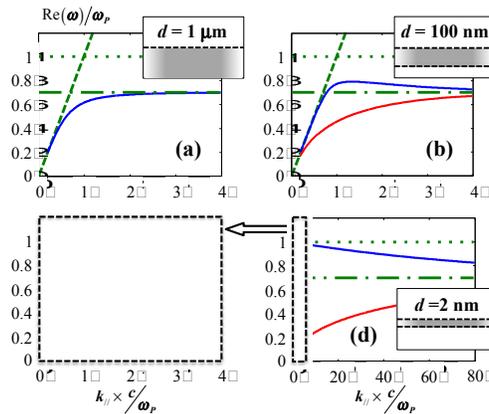
Fig. 2. (a) SPP supported by a layer with thickness of 1 μm, a value much larger than the skin depth. (b) The SPP splits into short-range (red) and long-range (blue) SPPs when the layer thickness is 100 nm, a value comparable to the skin depth. (c) Further decreasing the thickness to 2 nm, a value much smaller than the skin depth, a flat dispersion appears at $\omega/\omega_P=1$ that is associated to an ENZ mode. In (a)-(c), the dotted and dashed-dotted horizontal green lines depict the limits $\omega/\omega_P=1$ and $\omega/\omega_P=1/\sqrt{2}$, respectively. The dashed green line depicts the light line. (d) As in (c), showing a wider range of $k_{//}$.

It is straightforward to derive the asymptotic behavior for large $k_{//}$. When $k_{//} \to \infty$ we know that $k_{z1} = ik_{//}\sqrt{1 - \dfrac{\omega^2}{c^2 k_{//}^2}} \approx ik_{//}\sqrt{1 - \dfrac{\omega_P^2}{c^2 k_{//}^2}} \approx ik_{//}$, and the same approximation can be made for k_{z2}. It follows that for $k_{//}d \to \infty$, Eq. (1) leads to $\varepsilon_2 \to -1$ and $\omega \to \dfrac{\omega_P}{\sqrt{2}} - i\dfrac{\gamma}{2}$. To understand now the conditions under which an ENZ mode can be defined and what its peculiar features are, we have to rewrite Eq. (1) when ω is close to ω_P. For small values of the thickness such that $|k_{z2}d| \ll 1$, Eq. (1) can be rewritten as

$$2\varepsilon_2 k_{z1} = id\left(\varepsilon_2^2 k_{z1}^2 + k_{z2}^2\right) \qquad (2)$$

Noting again that $k_{z1} \approx ik_{//}$, Eq. (2) can be rewritten as

$$2\varepsilon_2 k_{//} = d\left[\frac{\omega^2}{c^2}\varepsilon_2(\varepsilon_2 + 1) - k_{//}^2\left(\varepsilon_2^2 + 1\right)\right] \approx -dk_{//}^2\left(\varepsilon_2^2 + 1\right) \qquad (3)$$

The second equality in Eq. (3) can be assumed if $\dfrac{\omega^2}{c^2}\varepsilon_2 \ll k_{//}^2$. Such a condition can be satisfied if $\varepsilon_2 \to 0$. This is possible for $\omega \approx \omega_P$; in such a case, we can rewrite Eq. (3) as $\left(\omega^2 + i\gamma\omega\right)\left(1 + \dfrac{k_{//}d}{2}\right) = \omega_P^2$ by neglecting the ε_2^2 term on the right-hand side. Under this approximation, a new dispersion relation can be derived for the ENZ mode:

$$\omega \approx \omega_P\left[1 - \frac{k_{//}d}{4}\right] - i\frac{\gamma}{2} \qquad (4)$$

This approximation is valid only when $\omega \approx \omega_P$. This equation is very similar to the approximation reported in [24] for the surface plasmon mode at a metallic surface with spatial dispersion. The existence domain of an ENZ mode is thus $\dfrac{\omega_P}{c} < k_{//} \ll \dfrac{4}{d}$. For instance, Fig. 3 shows the dispersion of the real and imaginary parts of ω of the long-range SPP for a layer thickness of 10 nm. In agreement with the previously defined domain, it is seen that the dispersion given by Eq. (4) (dashed black line) approximates quite well the real dispersion curve (solid blue line) in the region $\dfrac{\omega_P}{c} < k_{//} < \dfrac{1}{10}\dfrac{4}{d}$ (gray shaded area) giving a phenomenological approximation of the previous inequality $k_{//} \ll \dfrac{4}{d}$. Moreover, using field-continuity conditions dictated by Maxwell's equations, it has been shown in previous studies that the *z*-component of the electric field is much stronger than the in-plane components, and that the electric field exhibits a constant field profile within the slab [8]. This last feature is observed only in the range indicated by the grey shaded area in Fig. 3. It turns out that the ENZ mode can appear only for small thicknesses given by $\dfrac{2\pi}{\lambda_P} \ll \dfrac{1}{10}\dfrac{4}{d}$ (where $\lambda_P = \dfrac{2\pi c}{\omega_P}$ is the plasma wavelength), corresponding to a relative difference between ω and ω_P of less than 10%. A good rule of thumb is that the ENZ mode becomes apparent for nanoscale thickness $d \lesssim \dfrac{\lambda_P}{50}$ (in our case, $d \lesssim 20\text{nm}$). This explains why the ENZ mode was never observed in metals (λ_P on the order of hundreds of nanometers), but for example in doped semiconductors (λ_P on the order of 5 to 50 micrometers) where this condition can be easily met.
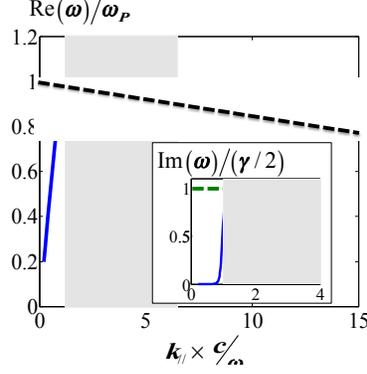
Fig. 3. The dispersion of the long-range (blue) SPP when the layer thickness is 10 nm. The dashed black line depicts the approximation $\text{Re}(\omega) \approx \omega_P\left[1 - \frac{k_{//}d}{4}\right]$. The shaded gray area depicts the range of $k_{//}$ below Eq. (4). The inset shows the imaginary part of the mode dispersion, which becomes constant and equals to $\gamma/2$ for large $k_{//}$. These losses equal the well-known losses of the short-range SPP.

Next, we show in Fig. 4 the dispersion of the real part of ω of the long-range SPP for three layer thicknesses, namely 2, 20, and 150 nm. Together with the dispersion diagrams, we also show the profile of the intensity of the z-component of the electric field versus the spatial variable z normalized by the thickness d and computed at $k_{//} = 2\omega_P/c$. We observe that when the dispersion curve falls within the existence range of the ENZ mode depicted by the shaded grey area, the field is rather constant within the slab. On the contrary, as shown in Fig. 4(c), the field exhibits a minimum in the middle of the slab if the dispersion is outside of the ENZ mode existence limits: this is the long range SPP behavior that has been known for decades for thin films. As predicted above, we see in Fig. 4 that an ENZ mode is observed only if $d <\approx 20\,\text{nm}$.
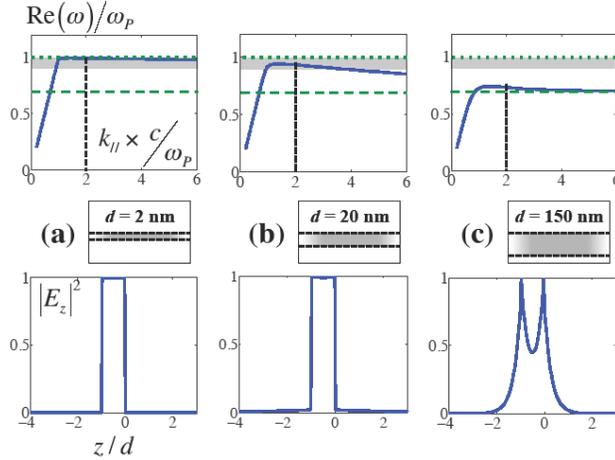
Fig. 4. (a). Dispersion (top) and profile of the intensity of the z-component of the electric field versus the spatial variable z normalized by the thickness d (bottom) computed at $k_{//} = 2\omega_P/c$ for the long-range SPP supported by a 2nm-thick layer surrounded by free space. The shaded gray area describes the ENZ mode validity range. (b)-(c) As in (a), for a slab thickness of 20 and 150 nm, respectively. $|E_z|^2$ is normalized to the maximum value. When the dispersion curve does not lie within the ENZ mode validity range, the field is not constant inside the layer.

Because larger fields are expected in thinner films, our next objective is now to derive the dependence of the electric field on the thickness of the film. We first compute the Poynting vector along the x direction

$$\langle S_x \rangle = \frac{1}{2}\text{Re}\left(-E_z H_y^*\right) = \frac{1}{2}\frac{\varepsilon_0}{k_{//}}\text{Re}\left(\omega^* \varepsilon_2^*\right)|E_z|^2 \qquad (5)$$

It is possible to show that $\text{Im}(\varepsilon_2) = 0$ for the complex frequency of the mode, so that $\text{Re}(\omega^* \varepsilon_2^*) = \text{Re}(\omega)\text{Re}(\varepsilon_2)$,

with $\text{Re}(\omega) = \omega_P\left(1 - \dfrac{k_{//}d}{4}\right) \approx \omega_P$ and $\text{Re}(\varepsilon_2) \approx 1 - \dfrac{\omega_P^2}{\text{Re}(\omega)^2} \approx \dfrac{2(\omega - \omega_P)}{\omega_P} = \dfrac{-k_{//}d}{2}$, leading to $\langle S_x \rangle = -\dfrac{\varepsilon_0 \omega_P d}{4}|E_z|^2$.

Now, due to the fact that the ENZ mode exhibits constant $|E_z|$, we integrate along the z axis to obtain

$$\int_z \langle S_x \rangle \approx \int_{-d}^{0} -\frac{\varepsilon_0 \omega_P d}{4}|E_z|^2 dz = -\frac{\varepsilon_0 \omega_P}{4}|E_z|^2 d^2 \tag{6}$$

The electric field is normalized in such a way that the mode carries 1 Watt of power per meter of wavefront, i.e. $\left|\int_z \langle S_x \rangle\right| = 1\,\text{W/m}$ [25]. This leads then to $|E_z|^2 \approx \dfrac{4}{\varepsilon_0 \omega_P d^2}$, or $E_z \propto \dfrac{1}{d}$. This linear dependence with $\dfrac{1}{d}$ is shown in

Fig. 5(a) where the magnitude of the z-component of the electric field (blue crosses) is computed at the center of the slab as a function of thickness. Figure 5(b) represents the magnitude of the z-component of the electric field versus the spatial variable z for different thicknesses d. As predicted, we observe a field increase of 10 times when comparing the 2 nm case to the 20 nm one. The linear dependence mentioned above can also be inferred by the results shown in [26].
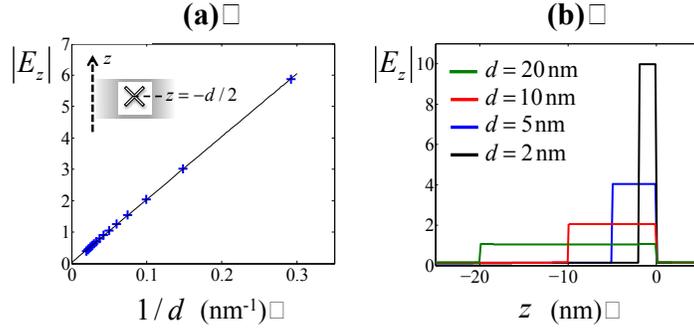
Fig. 5. (a). The magnitude of the z-component of the electric field dependence on the inverse of the layer thickness, calculated at the center of the slab as detailed in the inset and computed at $k_{//} = 2\omega_P/c$. The black line represents a linear fit of the crosses. (b) Magnitude of the z-component of the electric field versus the spatial variable z for various slab thicknesses. The lower the thickness is, the larger the field generated within the slab. In both figures, the electric field is normalized to the value exhibited for a thickness $d = 20$ nm.

Up to now, we have analyzed Drude layers in free space. If we were to assume the surrounding media to be dielectrics with permittivities $\varepsilon_1 = \varepsilon_3$, and still assuming $\varepsilon_2(\omega) = 1 - \dfrac{\omega_P^2}{\omega^2 + i\gamma\omega}$, it is easy to demonstrate that the approximate ENZ mode dispersion would become $\omega \approx \omega_P\left[1 - \dfrac{\varepsilon_1 k_{//}d}{4}\right] - i\dfrac{\gamma}{2}$. We aim to show now that this result can be generalized if the thin layer permittivity does not follow a Drude model. For this reason, let us consider the structure studied in [8]. The thin film is a now a glass layer, which can support an ENZ mode close to the longitudinal phonon frequency. The layer is deposited on a gold substrate and the upper medium is free space. All the material parameters are provided in [8] ($\lambda_P = 8\,\mu m$). In the ENZ mode regime, the dispersion relation remains linear (not shown here, see [8]). The dispersion slope $\Delta\text{Re}(\omega)/\Delta k_{//}$ is reported in Fig. 6 versus thickness d. It is seen that this slope has a linear dependence on d, suggesting that the properties analyzed earlier can be generalized to any structure supporting an ENZ mode. More generally, Fig. 6 suggests that the ENZ mode dispersion relation can always be written as $\omega \approx \omega_P[1 - \alpha \times k_{//}d] - i\dfrac{\gamma}{2}$, with α being a coefficient that depends on the permittivities of the semi-infinite media 1 and 3.
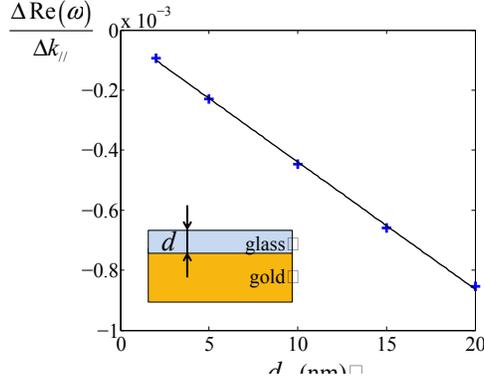
Fig. 6. Slope of the ENZ mode dispersion versus d computed for different thicknesses d for the structure in the inset.

From a practical point of view, these findings allow us to give some rule of thumb on material systems that can support ENZ modes. We map in Fig. 7 the ENZ wavelength (zero crossing of the permittivity, obtained for example in plasmonic or films supporting optical phonons) λ_P versus thin layer thickness d for some (non-exhaustive) material systems, and overlap colored boxes for each material system representing the experimentally achievable thickness. Thicker films are possible, but for example there are experimental lower bounds to the thickness of metals where they can still maintain good properties. The red dashed line depicts the thickness threshold, under which the ENZ mode can exist. From this figure, we conclude that the ENZ modes can be observed mainly in oxides, doped semiconductors, and polar materials, but not in metals, due to the combination of values of plasma wavelength and experimentally achievable thicknesses.
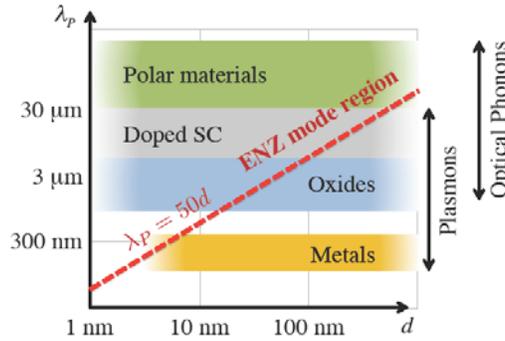
Fig. 7. Classification of some (non-exhaustive) material systems that may support ENZ modes, obtained by mapping the plasma wavelength λ_P versus thin layer thickness d. The color boxes for each material system extend horizontally and to the left to the minimum experimentally achievable thickness. The red dashed line defines the relation $\lambda_P = 50d$, which represents a boundary to determine if the structure supports an ENZ mode (left area).

The so-called ENZ mode has been discovered and used in pioneering papers [8,16,27]. Although the main features of this mode – almost-flat dispersion relation and large electric field in the thin layer – were briefly described, a complete study of this mode, including its domain of existence in for a general layered structure, was still missing. To the best of our knowledge, we have reported in this paper the first thorough description of this promising mode. In the simple case of a thin Drude nanolayer surrounded by free space, we have demonstrated that the ENZ mode is definitely a part of a long-range surface wave mode, which is characterized by a very large and almost constant electric field in the film. The electric field is inversely proportional to the thickness of the film. We have derived a useful form of the dispersion relation for this mode, leading to a simple definition of the frequency/wavevector range in which this mode can exist. This has allowed us to determine the range of thicknesses for which a film can support such a mode, and has provided us with a rule of thumb to understand which material systems can support an ENZ mode. We have further shown that the behaviors given by this very simple case are rather robust, since we can find the same behaviors in very different geometries and for different materials. This paves the way to very interesting possibilities, particularly in semiconductors, in which such ultrathin layers can be easily fabricated, and opens up possibilities in many applications, such as directional perfect absorption [19,28,29],

ultrafast voltage-tunable strong coupling with metamaterials [27], electro-optical modulation [30], and ultrafast thermal emission [16,31].

Acknowledgements

References
[1] K. L. Kliewer and R. Fuchs, Physical Review **150**, 573 (1966).
[2] D. Sarid, Physical Review Letters **47**, 1927 (1981).
[3] E. N. Economou, Physical Review **182**, 539 (1969).
[4] J. M. Pitarke, V. M. Silkin, E. V. Chulkov, and P. M. Echenique, Journal of Optics A: Pure and Applied Optics **7**, S73 (2005).
[5] R. P. Godwin and M. M. Mueller, Appl. Opt. **12**, 1276 (1973).
[6] D. W. Berreman, Physical Review **130**, 2193 (1963).
[7] B. Harbecke, B. Heinz, and P. Grosse, Applied Physics A **38**, 263 (1985).
[8] S. Vassant, J. P. Hugonin, F. Marquier, and J. J. Greffet, Opt Express **20**, 23971 (2012).
[9] A. D. Boardman, *Electromagnetic Surface Modes* (John Wiley & Sons, 1982).
[10] T. Taliercio, V. N. Guilengui, L. Cerutti, E. Tournié, and J.-J. Greffet, Opt. Express **22**, 24294 (2014).
[11] J. Bösenberg and H. Raether, Physical Review Letters **18**, 397 (1967).
[12] E. A. Vinogradov, G. N. Zhizhin, A. G. Mal'shukov, and V. I. Yudson, Solid State Communications **23**, 915 (1977).
[13] R. A. Ferrell, Physical Review **111**, 1214 (1958).
[14] A. Bichri, J. Lafait, and H. Welsch, Journal of Physics: Condensed Matter **5**, 7361 (1993).
[15] A. J. McAlister and E. A. Stern, Physical Review **132**, 1599 (1963).
[16] S. Vassant, A. Archambault, F. Marquier, F. Pardo, U. Gennser, A. Cavanna, J. L. Pelouard, and J. J. Greffet, Physical Review Letters **109**, 237401 (2012).
[17] N. Engheta, Science **340**, 286 (2013).
[18] M. Born and E. Wolf, *Principles of Optics: Electromagnetic Theory of Propagation, Interference, and Diffraction of Light* (Cambridge University Press, 1999).
[19] T. S. Luk *et al.*, Physical Review B **90**, 085411 (2014).
[20] D. M. Pozar, *Microwave Engineering* (John Wiley and Sons, 2011), 4th edn.
[21] A. Archambault, T. V. Teperik, F. Marquier, and J. J. Greffet, Physical Review B **79**, 195414 (2009).
[22] P. Berini, Adv. Opt. Photon. **1**, 484 (2009).
[23] S. A. Maier, *Plasmonics: Fundamentals and Applications* (Springer Science+Business Media LLC, New York, 2007).
[24] P. J. Feibelman, Physical Review B **40**, 2752 (1989).
[25] J. J. Burke, G. I. Stegeman, and T. Tamir, Physical Review B **33**, 5186 (1986).
[26] S. Campione, D. de Ceglia, M. A. Vincenti, M. Scalora, and F. Capolino, Physical Review B **87**, 035120 (2013).
[27] Y. C. Jun, J. Reno, T. Ribaudo, E. Shaner, J.-J. Greffet, S. Vassant, F. Marquier, M. Sinclair, and I. Brener, Nano Letters **13**, 5391 (2013).
[28] M. A. Badsha, Y. C. Jun, and C. K. Hwangbo, Optics Communications **332**, 206 (2014).
[29] S. Feng and K. Halterman, Physical Review B **86**, 165103 (2012).
[30] A. P. Vasudev, J.-H. Kang, J. Park, X. Liu, and M. L. Brongersma, Opt. Express **21**, 26387 (2013).
[31] S. Vassant, I. Moldovan Doyen, F. Marquier, F. Pardo, U. Gennser, A. Cavanna, J. L. Pelouard, and J. J. Greffet, Applied Physics Letters **102** (2013).